ELSEVIER

Polymer 43 (2002) 4769–4781

polymer

www.elsevier.com/locate/polymer

The interrelationship between processing conditions, microstructure and mechanical properties for injection moulded rubber-toughened poly(methyl methacrylate) (RTPMMA) samples

K. Porfyrakis[a], H.E. Assender[a,*], I.M. Robinson[b]

[a]*Department of Materials, University of Oxford, Parks Road, Oxford OX1 3PH, UK*
[b]*INEOS Acrylics UK Limited, P.O. Box 90, Wilton, Middlesbrough TS90 8JE, UK*

Received 19 April 2002; accepted 8 May 2002

Abstract

The interrelationship between processing conditions, developed microstructure and mechanical properties has been studied for a series of injection moulded rubber-toughened poly(methyl methacrylate) (RTPMMA) samples. A design of experiments (DOE) approach has been adopted to investigate the effect of barrel temperature, mould temperature, screw speed and back pressure on the mechanical properties of the mouldings. The back pressure has been identified as the single most important factor affecting the sample properties. Scanning electron microscopy (SEM), atomic force microscopy (AFM) and ultrasonic force microscopy (UFM) have been used to study the relationship between the rubber-toughened microstructure and mechanical properties. SEM has shown that the rubber particles are almost spherical in the central region of the injection-moulded samples, away from the sample surface. AFM topography measurements combined with UFM can reveal the distribution, elongation and orientation of the rubber particles close to the surface of the sample. UFM in particular reveals the core–shell structure of the particles as well as the presence of particles immediately under the surface, invisible by AFM. The particles are elongated in the skin region of the injection moulded samples and well aligned to the melt flow. UFM has shown that samples with different flexural properties exhibit a difference in the number and distribution of rubber particles present in the skin region.

Keywords: Rubber-toughened poly(methyl methacrylate); Processing; Microstructure

1. Introduction

Injection moulding is the dominant cyclic polymer processing technique. During each cycle, solid polymer in the form of powder or granules is fed through a feed hopper into a heated barrel that houses a reciprocating-screw. The polymer granules are melted and as the melt accumulates in front of the screw, it pushes the screw backward against a back pressure which can be set in advance. When sufficient amount of melt has been formed (equal to a dose), the screw is pushed forward like a ram and the melt is injected under very high pressures in a cavity (mould) where it solidifies, taking the shape of the cavity. The moulding is allowed to cool until beneath the glass transition of the polymer when it becomes mechanically stiff enough to be ejected from the mould. When a certain temperature beneath the glass transition has been reached the mould opens and the part is mechanically ejected. At the same time, a new injection dose is formed inside the barrel and the cycle is repeated. The cycle time depends on various factors but is usually in the range of several seconds to several minutes.

A large number of processing conditions control the injection moulding process including, barrel and mould temperatures, injection speed, hold pressure, back pressure, etc. Although much work has been published on the relationship between product morphology and property variations, the interrelationship between processing conditions, microstructure and mechanical properties has not yet been fully developed. The main reason is the complexity of the injection moulding process and the large number of possible parameter combinations that can be used to produce a moulded part. In addition, the literature is far from unanimous on the relationship between injection moulding conditions and final properties. For instance, Chiu and Hsieh [1] studied the correlation between the residual

* Corresponding author. Tel.: +44-1865-273781; fax: +44-1865-273789.
E-mail address: hazel.assender@materials.ox.ac.uk (H.E. Assender).

0032-3861/01/$ - see front matter
PII: S0032-3861(02)00286-0

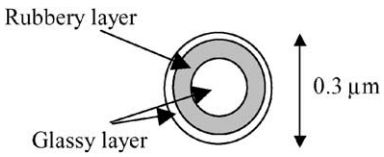

Fig. 1. Schematic diagram of a three-layer toughening particle, showing their size and internal structure. Rubber layers are displayed dark and glassy layers light.

stresses of ABS terpolymers and injection moulding conditions. It was found that the injection rate was the most important parameter affecting the level of residual stresses. On the other hand Akay and Ozden [2] having done similar work on ABS copolymers, concluded that it was only the mould temperature that appeared to have a significant effect on the residual stresses.

It becomes evident that the situation is even more complicated when rubber-toughened or fibre-reinforced polymers are involved, when the shape, orientation, deformation and distribution of fillers becomes important as shown by Ho et al. [3]. The aim of this work is to establish a link between processing conditions, developed microstructure and mechanical properties for a series of injection moulded rubber-toughened poly(methyl methacrylate) (RTPMMA) samples.

2. Experimental

2.1. Materials

The toughening particles consist of three radially alternating rubbery (poly[(*n*-butyl acrylate)-*co*-styrene]) and glassy (PMMA) layers, with the outer layer always being glassy. They were prepared by INEOS Acrylics using sequential emulsion polymerisation and were grown to a size of approximately 300 nm. The particles were cross-linked during their formation so that they maintain their morphology and size during blending with PMMA. Fig. 1 shows schematically the size and internal structure of a toughening particle.

The toughening particles were blended with the matrix PMMA by a single pass through a twin-screw co-rotating extruder (model CLEXTRAL BC21). The RTPMMA blends (25% per weight in rubber particles) were left to dry overnight and were then fed into the injection moulding machine.

2.2. Processing

An injection moulding machine (model DEMAG D40-151) was used to produce RTPMMA bars (120 mm × 10 mm × 4 mm). A design of experiments (DOE) method was used to perform a sequence of runs under different sets of processing conditions. The method is based on a 2^{k-1} fractional factorial design (where k is the number of processing variables) with two levels (high and low) of variation. The details of several DOE methods (including the factorial design) can be found elsewhere [4–6].

The processing variables that were considered during the injection moulding experiments are:

- barrel temperature,
- mould temperature,
- screw speed,
- back pressure.

The high and low values of each of the four processing parameters (factors) are shown in Table 1.

The runs that have been carried out in accordance to the 2^{4-1} fractional factorial design are shown in Table 2.

Roughly 60 samples were moulded for each run. Some of these samples were rejected (due to the presence of 'sink marks' or other defects) to ensure a reasonably uniform part quality.

2.3. Mechanical testing

2.3.1. Flexural test

Three-point bend flexure tests were carried out using an Instron (5544 model) machine in accordance with ISO 178. The thickness of the samples was approximately 4 mm. The three-point span was set to be at a 16:1 ratio of the thickness of each sample. The load was applied at a rate of 2 mm/min (cross-head speed). Five samples were tested from each run. Mean values for the flexural modulus (E) and flexural strength (yield stress, σ_y) have been calculated.

2.3.2. Impact tests

Notched Izod impact tests were conducted under a Ceast Izod impact machine in accordance with ISO 180. A band saw was used to cut samples of size: 63.5 mm × 10 mm × 4 mm. A broaching machine was used to prepare a notch at each test specimen (notch depth = 2 mm). Ten samples were tested from each run.

Unnotched Charpy impact tests were also carried out

Table 1
High, low and medium values of the processing parameters varied during the injection moulding experiments

	Barrel temperature (BT) (°C)	Mould temperature (MT) (°C)	Screw speed (SS) (rpm)	Back pressure (BP) (bar)
Low	200	40	100	5
High	250	60	300	15
Medium	225	50	200	10

Table 2
Sets of processing conditions used during injection moulding. The run no. 5 corresponds to the 'mid-point' where all variables have their mean values

Run no.	Barrel temperature (°C)	Mould temperature (°C)	Screw speed (rpm)	Back pressure (bar)
1	200	40	100	5
2	200	40	300	15
3	200	60	100	15
4	200	60	300	5
5	225	50	200	10
6	250	40	100	15
7	250	40	300	5
8	250	60	100	5
9	250	60	300	15

under a Ceast Charpy impact machine in accordance with ISO 179. A band saw was used to cut samples to a length of 80 mm. Ten samples were tested from each run. Mean notched Izod and unnotched Charpy impact strength values have been calculated.

2.4. Surface characterisation

2.4.1. Scanning electron microscopy (SEM)

The fracture surfaces of the injection moulded RTPMMA specimens were studied using a Hitachi™ S 520 Scanning Electron Microscope. The samples were gold coated in advance using an E5400 sputter coater to provide an electrically conductive surface layer. A voltage of 10 kV was used due to the sensitivity of PMMA to the electron beam. Magnification exceeding 15000 ×, producing sub-micron resolution, was possible.

2.4.2. Atomic force microscopy (AFM) and ultrasonic force microscopy (UFM)

Specimens from the injection moulded samples were used for AFM and UFM characterisation, in order to investigate the morphology close to the surface. A Park Scientific Instruments autoprobe™ CP atomic force microscope was used to acquire AFM topography images. Park Scientific™ Silicon and gold-coated triangular ultralevers were used (types UL 06 B and UL 06 A, respectively). Their properties are shown in Table 3. An in-depth review of the AFM technique and its application to polymer surfaces can be found elsewhere [7,8].

The autoprobe™ CP has been modified in order to acquire the UFM signal simultaneously with topography.

Table 3
Mechanical characteristics of the cantilevers used for AFM and UFM

Cantilever type	UL 06 A	UL 06 B
Cantilever length (μm)	180	180
Cantilever width (μm)	18	38
Cantilever thickness (μm)	0.6	1
Radius of curvature (nm)	<50	10
Force constant (N/m)	0.05	0.40
Resonant frequency (kHz)	22	45

The samples were mounted on a ceramic piezotransducer using a thin layer of crystalline salol (phenyl salicylate) before mounting on the AFM. Vibrations with frequencies up to several MHz were excited in the sample. The tip does not vibrate with the sample but it is cyclically indented into the sample resulting in an additional 'ultrasonic force' on the cantilever. The contrast of the UFM therefore depends upon the elastic and adhesive properties of the surface. The UFM technique is discussed in detail elsewhere [9–19].

AFM and UFM have produced very informative images of the surface microstructure, however they are not so effective when studying fracture surfaces; SEM is more suitable for this purpose.

3. Results and discussion

3.1. Mechanical testing results

The mechanical testing results are summarised in Table 4. Fig. 2 shows the flexural properties of the injection moulded bars produced under different runs. Their impact properties are shown in Fig. 3. In all cases mean values are presented. In Figs. 2 and 3 standard deviation limits are also shown.

3.2. Analysis of designed experiments using best subsets regression methods

The experimental data has been fully analysed statistically. The regression analysis has been performed using the statistics analysis package MINITAB™.[1]

Regression analysis investigates the relationship between a response variable and one or more predictor variables. The simplest regression model is the *linear regression model*, defined by the *regression equation*:

$$\text{Response} = \text{constant} \pm (\text{Coeff.}_1 \times \text{Predictor}_1) \pm (\text{Coeff.}_2 \times \text{Predictor}_2) \pm \cdots + \text{error} \quad (1)$$

[1] Release 11 (Minitab Inc., 3081 Enterprise Drive State College, PA 16801-3008, USA).

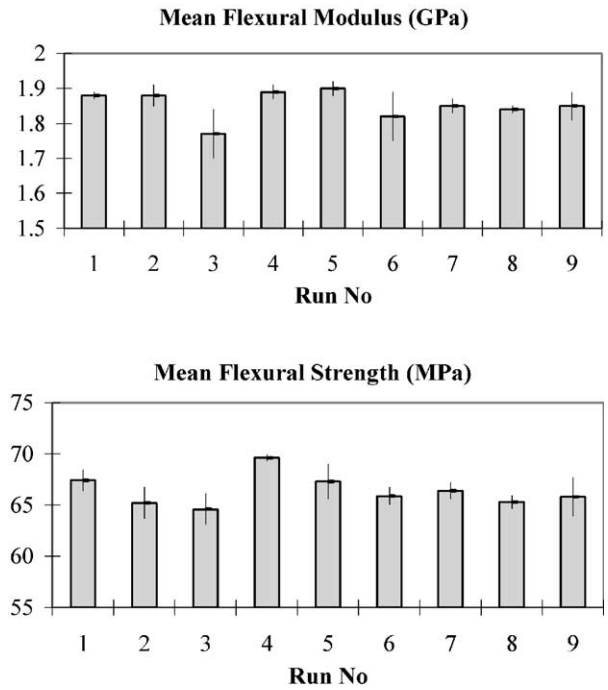

Fig. 2. Mean flexural modulus and flexural strength for the injection moulded samples.

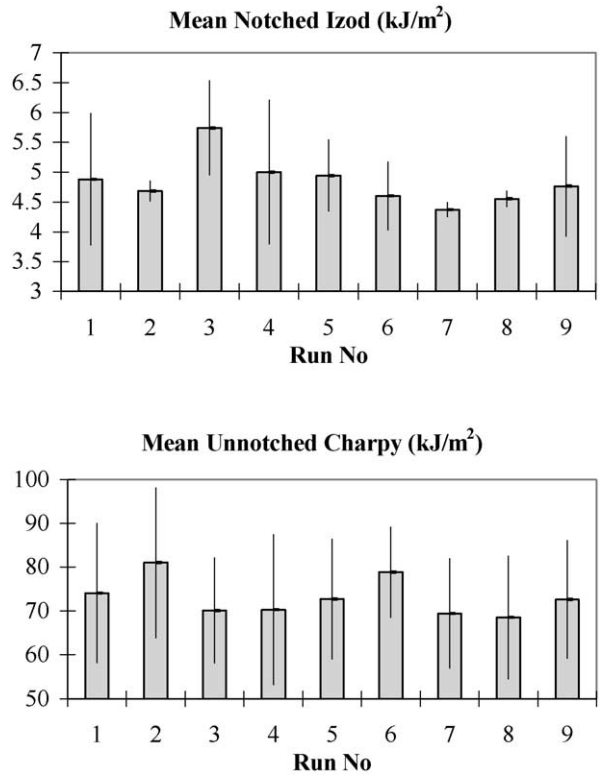

Fig. 3. Mean notched Izod and unnotched Charpy impact strengths for the injection moulded samples.

Full regression analysis requires the fitting of every possible regression equation that involves any possible combination of the predictor variables, requiring, e.g. 2^{10} equations for 10 variables to be examined. A practicable alternative to performing all regressions is to select a model with the 'best' subset of variables by selecting the smallest subset that fulfils certain statistical criteria in defining the relationship between response variables and one or more predictors. Certain statistics are generated for each model: the maximum R^2_{adjusted} and C_p. These are defined more fully later. When comparing models with different number of predictors, choosing the model with the highest R^2_{adjusted} is equivalent to choosing the model with the smallest mean square error. Consequently we seek the model with the highest R^2_{adjusted} combined with the best value of C_p (i.e. closely fitting the number of variables introduced into the regression equation). This strategy represents a balance between explaining the underlying data set whilst not over fitting, thus maintaining predictability.

R^2_{adjusted} is an approximately unbiased estimate of the population R^2 (adjusted for degrees of freedom of the dataset), and is calculated by the formula

$$R^2_{\text{adjusted}} = 1 - [(\text{Sum of squares error})/(n-p)]/[(\text{Total sum of squares})/(n-1)] \quad (2)$$

where n is number of data points (in our case n is equal to the number of runs, i.e. $n = 9$) and p is the number of coefficients fit in the regression equation (p = number of

Table 4
Summary of the mean values for the flexural modulus (E), flexural stress (σ_y), notched Izod (NI) and unnotched Charpy (UNC) mechanical tests for the various sample conditions with barrel temperature (BT), mould temperature (MT), screw speed (SS) and back pressure (BP) either high (H), medium (M) or low (L) (see Table 1)

Run	E (GPa)	σ_y (MPa)	NI energy (kJ/m^2)	UNC energy (kJ/m^2)	BT	MT	SS	BP
1	1.88	67.4	4.88	74.1	L	L	L	L
2	1.88	65.2	4.68	81.0	L	L	H	H
3	1.77	64.6	5.74	70.1	L	H	L	H
4	1.89	69.6	5.00	70.3	L	H	H	L
5	1.90	67.3	4.94	72.7	M	M	M	M
6	1.82	65.9	4.60	78.8	H	L	L	H
7	1.85	66.4	4.37	69.4	H	L	H	L
8	1.84	65.3	4.55	68.5	H	H	L	L
9	1.85	65.8	4.76	72.6	H	H	H	H

Table 5
Regression analysis for the flexural modulus results

Variables in regression	$R^2_{adjusted}$ (%)	C_p	Barrel temperature	Mould temperature	Screw speed	Back pressure
1	13.4	1.3			X	
1	6.9	1.8				X
2	23.7	1.8			X	X
2	7.1	2.8		X	X	
3	18.2	3.3		X	X	X
3	13.9	3.5	X		X	X
4	4.5	5.0	X	X	X	X

predictor variables plus the intercept). The C_p statistic is given by the formula

$$C_p = \left(\frac{\mathrm{SSE}_p}{\mathrm{MSE}_m}\right) - (n - 2p) \quad (3)$$

where SSE_p is sum of squares error for the best model with p parameters, and MSE_m is the mean square error for the model with all m predictors (in our case $m = 4$).

If the model is adequate (i.e. fits the data well), then the expected value of C_p is approximately equal to p, the number of parameters in the model. A small value of C_p indicates that the model is relatively precise (has small variance) in estimating the true regression coefficients and predicting future responses. This precision will not improve much by adding more predictors. Models with considerable lack of fit have values of C_p larger than p.

The regression equations formed by such an analysis serve a technological purpose in describing the likely outcome of desired variables from predictors under similar operating conditions. The equations do not define at a fundamental level how the operating conditions affect the variables concerned, but they do offer guidance in optimising operating conditions for practical use. This is often all that is required to operate successfully. It is extremely difficult to translate basic scientific understanding into machine settings on a piece of melt processing equipment, whereas the simple regression analysis quickly points to optimum conditions. However science provides insights, which allow optimisation outside the operating conditions under consideration in the designed experiment, and so a wise course of action is to combine pragmatic optimisation via designed experiments with fundamental scientific know-how.

With this in mind, a best subsets regression analysis of the four principal response variables under study (flexural modulus and strength, notched Izod and unnotched Charpy impact strength) is presented here. The pattern of the analysis is to select the best set of processing variables for each measured mechanical property using best subsets regression analysis, to create the regression equation and then to predict the values for the operating conditions described in Table 2. For each of the regression equations formed, the values for barrel and mould temperature are in degrees centigrade, the screw speed refers to rpm and the back pressure is given in kbar. The empirical regression relationships could also serve as predictions for the other half of the experimental design (where we would simply reverse the conditions between high and low settings in Table 2).

3.2.1. Analysis of flexural modulus results

Analysing the data contained in Tables 2 and 4 for flexural modulus using best subsets regression analysis produces Table 5. Table 5 presents the 'best two' subsets for the dataset. In other words, rows one and two present the best two equations containing one variable, rows three and four present the best two equations containing two variables and so on. The variables marked by X in the table denote terms entered into the regression equation. The same pattern is followed in all subsequent regression results.

The terms selected for further analysis are screw speed and back pressure since they have the highest $R^2_{adjusted}$ and a C_p value relatively close to the number of variables in regression analysis. For example, the regression analysis equation for the flexural modulus proposed is:

$$E(\mathrm{GPa}) = 1.85 + 0.0002\ \text{Screw speed} - 0.0035\ \text{Back pressure} \quad (4)$$

Eq. (4) indicates that back pressure is a particularly important variable, as will be shown later. Comparison between the experimental and predicted values (from the regression analysis) of the flexural modulus results is shown in Table 6.

3.2.2. Analysis of flexural strength results

Analysing the data contained in Tables 2 and 4 for flexural strength using best subsets regression analysis produces Table 7.

The terms selected for further analysis are the barrel temperature and back pressure since they have a high $R^2_{adjusted}$ and a C_p value close to the number of variables in regression analysis. The regression analysis equation for the

Table 6
Comparison between the experimental and predicted (from the regression analysis) values of the flexural modulus results

Run	E (GPa)	
	Experimental	Predicted
1	1.88	1.85
2	1.88	1.86
3	1.77	1.82
4	1.89	1.89
5	1.90	1.85
6	1.82	1.82
7	1.85	1.89
8	1.84	1.85
9	1.85	1.86

flexural strength proposed is:

$$\sigma_y(\text{MPa}) = 67.2 + 0.00475\ \text{Screw speed} - 0.18\ \text{Back pressure} \quad (5)$$

Notice these are the two same variables indicted in the analysis of the flexural modulus, with the trend for each property with conditions the same. Comparison between the experimental and predicted values (from the regression analysis) of the flexural modulus results is shown in Table 8.

3.2.3. Analysis of notched Izod impact strength results

Analysing the data contained in Tables 2 and 4 for notched Izod impact strength using best subsets regression analysis produces Table 9.

The terms selected for further analysis are the barrel temperature, mould temperature and back pressure since they have the highest R^2_{adjusted} and a C_p value fairly close to the number of variables in regression analysis. The regression analysis equation for notched Izod fracture energy proposed is:

$$\text{NI}\ (\text{kJ/m}^2) = 5.91 - 0.0101\ \text{Barrel temperature} + 0.019\ \text{Mould temperature} + 0.0245\ \text{Back pressure} \quad (6)$$

Comparison between the experimental and predicted values (from the regression analysis) of the flexural modulus results is shown in Table 10.

Table 8
Comparison between the experimental and predicted (from the regression analysis) values of the flexural strength results

Run	σ_y (MPa)	
	Experimental	Predicted
1	67.4	66.8
2	65.2	66.0
3	64.6	65.0
4	69.6	67.8
5	67.3	66.4
6	65.9	65.0
7	66.4	67.8
8	65.3	66.8
9	65.8	66.0

3.2.4. Analysis of unnotched Charpy impact strength results

Analysing the data contained in Tables 2 and 4 for unnotched Charpy impact strength using best subsets regression analysis produces Table 11.

The terms selected for further analysis are the mould temperature and back pressure since they have the highest R^2_{adjusted} and a C_p values matching closely the number of variables in regression analysis. The regression analysis equation for the unnotched Charpy fracture energy proposed is:

$$\text{UNC}\ (\text{kJ/m}^2) = 81.6 - 0.272\ \text{Mould temperature} + 0.505\ \text{Back pressure} \quad (7)$$

Comparison between the experimental and predicted values (from the regression analysis) of the flexural modulus results is shown in Table 12.

3.3. Key processing variables and their effect on mechanical properties

From the above analysis, the following observations can be made on the effect of processing conditions on mechanical properties.

Mould temperature influences the two measures of

Table 7
Regression analysis for the flexural strength results

Variables in regression	R^2_{adjusted} (%)	C_p	Barrel temperature	Mould temperature	Screw speed	Back pressure
1	27.5	0.5				X
1	0.0	2.6			X	
2	26.2	1.7			X	X
2	23.6	1.8	X			X
3	23.9	3.0	X		X	X
3	11.9	3.7		X	X	X
4	5.1	5.0	X	X	X	X

Table 9
Regression analysis for the notched Izod impact strength results

Variables in regression	$R^2_{adjusted}$ (%)	C_p	Barrel temperature	Mould temperature	Screw speed	Back pressure
1	32.7	9.1	X			
1	12.3	13.4		X		
2	52.5	5.5	X	X		
2	34.3	8.8	X			X
3	58.4	5.2	X	X		X
3	57.8	5.3	X	X	X	
4	66.6	5.0	X	X	X	X

Table 10
Comparison between the experimental and predicted (from the regression analysis) values of the notched Izod impact strength results

Run	NI (kJ/m^2)	
	Experimental	Predicted
1	4.88	4.78
2	4.68	5.02
3	5.74	5.40
4	5.00	5.16
5	4.94	4.84
6	4.60	4.52
7	4.37	4.27
8	4.55	4.65
9	4.76	4.90

toughness (notched Izod and unnotched Charpy), probably by altering the degree of residual stress present in the samples and the amount of orientation achieved in the impact modifiers themselves at the surface of the samples. It can be seen from Eqs. (6) and (7) that the mould temperature modifies the notched Izod impact strength and unnotched Charpy impact strength in opposite fashions. This can be accounted for by consideration of the residual thermal stress distribution, which is approximated using the following expression [20]

$$\sigma_x = \alpha E T_o (1/3 - (y/c)^2) \quad (8)$$

where α is the thermal expansion coefficient, E, the Young's modulus, T_o, the difference between the temperature of the surface of the mould and the temperature which the polymer solidifies (T_g), $2c$, the width of the sample and y is the position through the sample thickness, varying from $-c$ to $+c$.

Consequently, increasing T_o by reducing the mould temperature increases the compressive stresses at the surface of the sample and the tensile stresses in the interior of the sample. We might anticipate, using this simple analysis, that extra compressive stresses in the surface regions of test samples resulting from low mould temperature would help boost the unnotched Charpy result. The opposite might be anticipated for notched Izod samples, as these samples are prepared by machining the surface layers away to produce a semi-sharp notch radius. Consequently, the stress concentration towards the centre of the sample may have more influence on the notched Izod results. Thus decreasing the mould temperature should increase the tensile stress present in the centre of the sample (decreasing the notched Izod result). The expected patterns for these simple toughness tests with residual thermal stresses are experimentally observed as the mould temperature is increased or decreased.

Barrel temperature affects the notched Izod impact strength. Increasing the barrel temperature reduces the melt viscosity and consequently leads to increased melt elongation of the impact modifiers. This is in agreement with the reduced notched Izod impact strength value that is observed (Eq. (6)).

Screw speed affects the flexural modulus and strength directly, that is increasing the screw speed increases the stiffness and strength. This is also possibly a rheological effect.

Back pressure influences all four variables (flexural

Table 11
Regression analysis for the unnotched Charpy impact strength results

Variables in regression	$R^2_{adjusted}$ (%)	C_p	Barrel temperature	Mould temperature	Screw speed	Back pressure
1	31.6	5.9		X		
1	25.1	7.0				X
2	66.1	1.6		X		X
2	24.5	7.4	X	X		
3	64.6	3.1	X	X		X
3	59.8	3.6		X	X	X
4	56.3	5.0	X	X	X	X

Table 12
Comparison between the experimental and predicted (from the regression analysis) values of the unnotched Charpy impact strength results

Run	UNC (kJ/m^2)	
	Experimental	Predicted
1	74.1	73.3
2	81.0	78.3
3	70.1	72.9
4	70.3	67.8
5	72.7	73.1
6	78.8	78.3
7	69.4	73.3
8	68.5	67.8
9	72.6	72.9

modulus, flexural strength, notched Izod impact strength and unnotched Charpy impact strength) where an assessment of mechanical integrity is concentrated in the skin region of the sample.

If one single most important factor has to be identified, then that would be the back pressure. High back pressure leads to good impact (via both test methods) but poor flexural properties and vice versa. As already mentioned, back pressure is the pressure that is exerted by the injection moulding machine to the screw as it retracts and the polymer melt accumulates in front of it.

The effect of the back pressure on the mechanical properties of a moulded article has not yet been thoroughly investigated. The vast majority of the scientific literature has focused on the effect of the melt and mould temperatures [2,21–23] and the injection flow rate [1,24,25]. However, Skourlis et al. [26] observed that the hold pressure was the most important single parameter affecting mechanical properties of advanced styrenic resins (rubber-toughened resins with structure similar to HIPS). Generally, the higher the hold pressure, the better the property is. Better packing of the chain molecules was proposed to be the reason for this behaviour.

The results published by Skourlis et al. [26] exhibit an interesting similarity with those presented in this work. Even though the hold pressure has a qualitative difference from the back pressure (hold pressure is the pressure applied during the cooling/packing stage of the melt) the back pressure could, in a similar way, affect the packing and orientation of the chain molecules. Furthermore, it is known that the bulk density of the polymer granules increases with pressure [27]. As a result the solid granules are compacted closer together during the plasticising stage when higher back pressure is applied. This could also contribute to better packing in the melt leading to better impact properties.

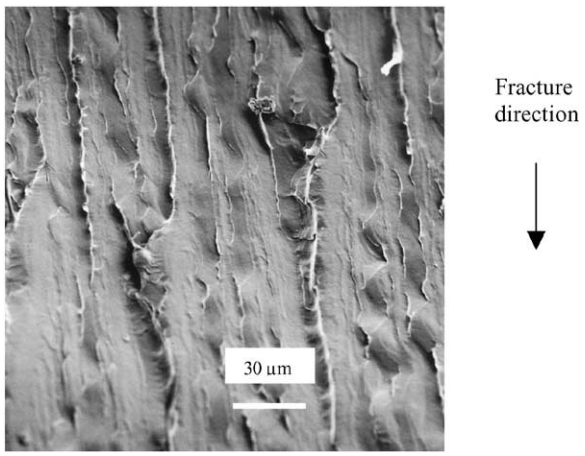

Fig. 4. SEM micrographs of the fracture surface of neat PMMA. The deformation mechanism appears to be crazing.

Notched Izod impact strength is also improved by a combination of low barrel, high mould temperatures and high back pressure. Low barrel temperature, in particular, leads to an increase in molecular orientation due to the fast cooling rates associated with it [28]. An increase in orientation improves significantly the notched Izod impact strength, measured across the flow.

Generally high impact resistance is accompanied by a low modulus and yield stress. Consequently, it does not come as a surprise that flexural properties are improved with lower back pressure and vice versa. Overall, run nos. 3 and 4 are the ones that appear to exhibit the largest difference in mechanical properties (except for the case of unnotched Charpy impact strength), as is summarised in Table 13.

For this reason samples from run nos. 3 and 4 were chosen for microscopy characterisation in order to closely investigate the effect of processing conditions on the microstructure (distribution and deformation of rubber particles) related to the mechanical properties of the final product.

3.4. SEM characterisation results

The samples chosen for SEM investigation were each notched and immersed in liquid nitrogen (to facilitate brittle failure) before being fractured. Fig. 4 shows a micrograph of the fracture surface of un-toughened PMMA. It can be seen

Table 13
Mechanical properties of the injection moulded samples for runs 3 and 4

Run no.	Flexural modulus (GPa)	Flexural strength (MPa)	Notched Izod (kJ/m^2)	Unnotched Charpy (kJ/m^2)
3 (standard deviation)	1.77 (0.07)	64.6 (1.5)	5.74 (0.79)	70.1 (12)
4 (standard deviation)	1.89 (0.02)	69.6 (0.31)	5.00 (1.21)	70.3 (17.1)
% difference between run nos. 3 and 4	6.8	7.7	14.8	0.3

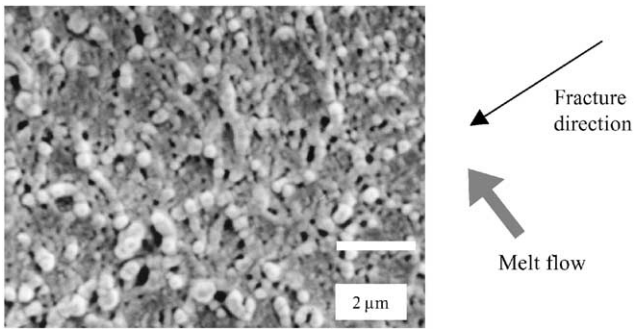

Fig. 5. SEM micrograph of a RTPMMA sample from run no. 3. The flow direction lies in the fracture plane, as indicated by the arrow.

that untoughened PMMA deforms by crazing. This behaviour is typical for a glassy thermoplastic such as PMMA [29,30].

SEM fractography of RTPMMA shows that the fracture surface of RTPMMA samples appears to be much rougher than that of neat PMMA. Holes and dome-like features of various sizes dominate the surface. Fig. 5 shows a micrograph of an injection moulded RTPMMA sample from run no. 3. The sample was cut out of a moulded bar after it was tested via the three-point bending test. The specimen was then fractured. Hence, the fracture surface visible in Fig. 5 originates from sample preparation. The melt flow direction lies in the fracture plane.

The main features of this micrograph are small cavities and larger spherical features. These spherical features are estimated to be around 300 nm in diameter whereas the cavities (appearing as dark spots) are smaller. It is therefore postulated that the visible spherical features are actually the rubber particles dispersed in the PMMA matrix, while the cavities represent positions that the particles used to occupy before they debonded. It appears that a large number of particles are well adhered to the matrix and the particles are well-dispersed since not many 'clusters' of particles are visible. The very rough surface and the 'strands' of matrix connecting the particles are signs that the matrix has undergone plastic deformation, which implies that shear yielding has occurred and it is a manifestation of ductile failure [31]. Similar micrographs were obtained from samples from run no. 4 when fractured under the same conditions.

Fig. 6 shows another micrograph of the fracture surface of an injection moulded sample from run no. 3. This time the sample was cut out of a moulded bar from the densely stress-whitened region of the bar after it was tested via the unnotched Charpy impact test. The melt flow direction lies in the fracture plane.

The micrographs shown in Figs. 5 and 6 exhibit substantial differences. The surface of the impact test sample (Fig. 6) is dominated by extensive cavitation. Only a few particles appear to be adhered to the matrix surface. Plastic deformation of the matrix is also visible. Additionally, the few particles that are still adhered to the surface

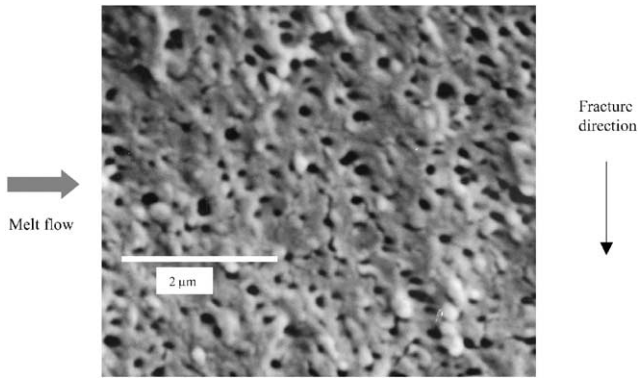

Fig. 6. SEM micrograph of a RTPMMA sample from run no. 3. The melt flow direction lies in the fracture plane. The sample originates from a bar tested by the unnotched Charpy impact test.

appear to be smaller in size (the average diameter is estimated to be less than 200 nm) compared to the particles of Fig. 5, which are roughly 300 nm in diameter. Therefore it could be argued that, what is visible as a spherical feature in the micrograph of Fig. 6, is not a 'whole' particle but a part of its internal structure (i.e. the glassy core with or without the internal rubbery layer). In other words, along with the apparent cavitation, the particles visible in Fig. 6 may have also undergone internal debonding. This conclusion is further supported by the fact that both samples of Figs. 5 and 6 originate from the same batch of RTPMMA material; hence one would expect the particles in the samples to be of similar size.

The extent of internal cavitation combined with the possible particle debonding (Fig. 6) could provide an explanation for the macroscopic difference (in the degree of stress-whitening) between the flexural test and impact test samples. No stress-whitening effect was observable in the region of the sample shown in Fig. 5. The particles are well adhered to the matrix. Since almost no volume increasing mechanism is present, no cavitation occurs; hence the sample does not scatter light effectively, remaining transparent. On the other hand, stress whitening seems to be promoted by particle cavitation and internal debonding,

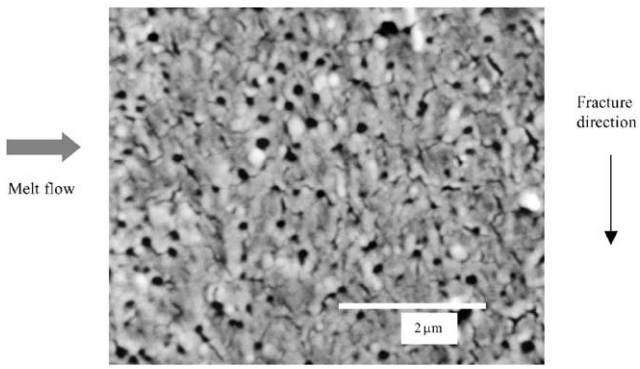

Fig. 7. SEM micrograph of a RTPMMA sample from run no. 4. The melt flow direction lies in the fracture plane. The sample comes from a bar tested by the unnotched Charpy impact test.

which in turn are promoted by the high loading rates encountered during the impact test.

Similar SEM investigation was carried out for the injection moulded samples from run no. 4. Fig. 7 shows a micrograph of the fracture surface of a sample that was cut out of a moulded bar after it was tested via the unnotched Charpy impact test. The melt flow direction again lies in the fracture plane.

The micrograph of Fig. 7 shows considerable similarities with that of Fig. 6. A large number of cavities are visible. Occasionally, spherical features can be observed. These features are thought to be internal particle structures (glassy core with or without the rubbery layer on top) for the same reasons presented earlier. Plastic deformation of the matrix is again present. It must be noted that the small cracks visible in most micrographs (with length in the range 0.3–1 μm) are probably caused by radiation damage and hence are formed by the imaging processes.

Overall, there is no significant difference in the unnotched Charpy impact strength between samples from run nos. 3 and 4 as shown. Indeed, the mean values for unnotched Charpy impact strength of samples from run nos. 3 and 4 were measured to be 70.1 and 70.3 kJ/m^2, respectively. Nevertheless, the impact strengths of the individual samples from run nos. 3 and 4 shown in Figs. 6 and 7, respectively, have been measured to be 72.62 and 62 kJ/m^2, respectively. This constitutes a difference of about 15%. In addition, there is a substantial difference in flexural strength of these samples. One would expect the above differences to be reflected in the microstructure of the respective fracture surfaces. Clearly, the difference in microstructure when a sample is fractured by different methods is manifested in Figs. 5 and 6. However this does not seem to be the case when different samples are fractured by the same method, as shown by comparison of Figs. 6 and 7. Therefore, analysis of the microstructure by SEM is found to be not always sufficient to account for differences in mechanical properties encountered in complex materials like RTPMMA. Combining SEM with another technique such as AFM or UFM can enhance characterisation.

3.5. AFM and UFM characterisation results

The surface of the injection-moulded bars has been mapped, using AFM and UFM, along their width and their length in an attempt to determine the shape, size and dispersion of the rubber particles. AFM images were not taken from the fracture surfaces, as they were too rough and hence unsuitable for AFM investigation. Figs. 8 and 11 show AFM (topography) and UFM images of samples from run no. 4.

The first conclusion one can draw is that the sample surface is not flat in the nanometre scale. AFM topography images reveal the presence of ‘bumps’ and cavities. These features are attributed to the presence of the rubber particles in the vicinity of the sample surface. This belief is indeed

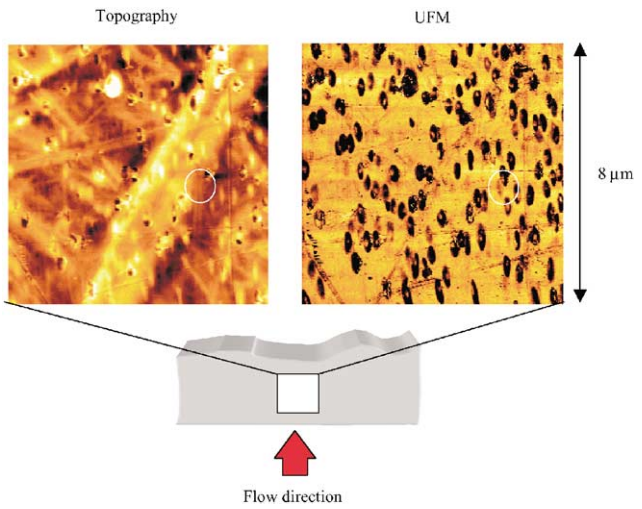

Fig. 8. AFM topography (left) and UFM (right) images on the surface of a moulding from run no. 4. The flow is vertical. The two images were taken simultaneously at the same position. The circle identifies an example of a rubber particle, as discussed in the text.

verified by UFM characterisation. UFM images give more information on the rubber-toughened microstructure due to the sensitivity of the technique to surface elastic and adhesive properties. In this case, because of the big difference in stiffness between rubber particles and PMMA matrix, it is believed that elastic properties provide main contribution to the UFM signal [19]. The compliant material appears darker while stiffer material appears brighter. UFM, with its ability to provide such a good contrast between the stiffer PMMA matrix and the softer rubber particles, has produced images of unprecedented detail for rubber-toughened acrylics.

UFM has shown that the rubber particles are well dispersed in the matrix; no significant particle agglomeration is visible. UFM images can also reveal the presence of rubber particles immediately under the surface, as shown at the position marked within the circle in Fig. 8. These particles are invisible in the AFM images. Hence, UFM can be used to probe the properties of the subsurface without any significant damage to the sample.

Fig. 8 clearly shows that the particles in the skin region are well oriented with the melt flow direction and quite elongated. This behaviour is dictated by the fountain flow phenomenon, which takes place in the vicinity of the flow front during the filling of the mould. There, the melt spills outward towards the walls. This flow pattern, combined with the high stresses and thermal gradients present, causes the rubber particles to elongate as they approach the cold walls [32]. Due to the low wall temperature, the melt solidifies rapidly creating a solid skin next to the walls. Hence, the particles are trapped retaining their shape and orientation as shown in Fig. 9.

As a result, three distinct regions are developed in the mould. Just underneath the surface, the particles are elongated and well aligned with the flow direction. As one

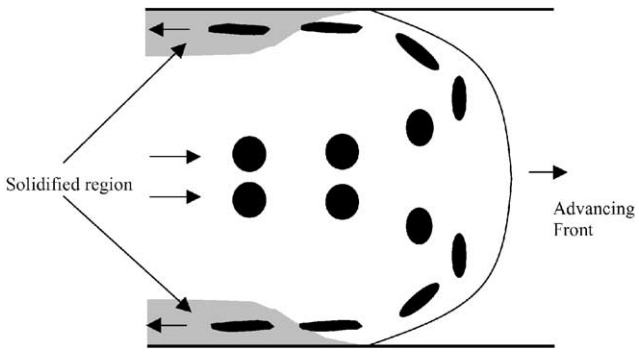

Fig. 9. Schematic illustration of the fountain flow phenomenon of polymer injection moulding showing the observed resulting elongation of the rubber particles close to the wall.

approaches the centre, the particles are oriented in an axis approximately 45° to the flow direction. This area is called the 'shear' region. Finally, in the central region the particles are more spherical and there is little evidence of orientation. The SEM micrographs shown in Figs. 6 and 7 were taken in the central region of the sample, between the shear regions. The presence of the 'shear' regions has also been verified by SEM, as shown in Fig. 10.

Height profile analysis of the AFM images at the mould surface of the sample has been carried out using the ProScan™ Image processing software in order to calculate the particles' contour and size. The amount the observed bump-like features project from the matrix typically varies from 40 to 150 nm. Elongation is quite intense, forming ellipsoidal particles. The eccentricity e of the projected ellipses varies from 0.70 to 0.95.

Similar AFM and UFM investigations have been carried out on the surface at the centre of the end of the injection moulded bars. Fig. 11 shows AFM and UFM images in this region, farthest from the gate at the end of the flow path, from run no. 4.

The average size of the particles can be estimated to be around 300 nm in diameter, which agrees with the value given by the manufacturer implying that the particles are approximately spherical, as we might expect and not ellipsoids that appear to be circular by projection. The

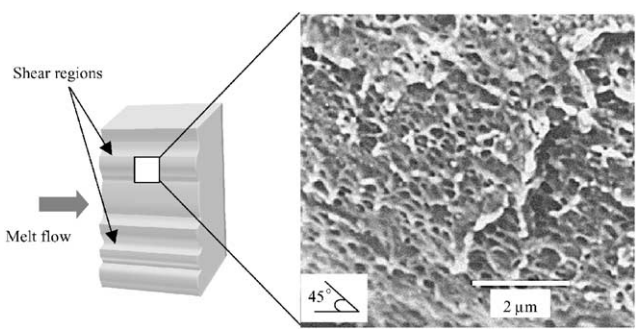

Fig. 10. Micrograph of the fracture surface of a sample from run no. 4 in the 'shear region'. The fracture plane is parallel to the flow direction. The particles appear to be oriented in an axis approximately 45° to the flow direction.

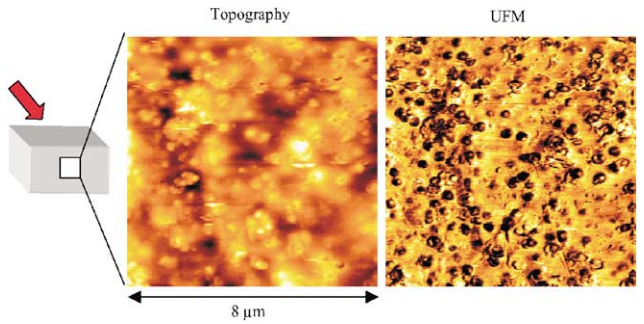

Fig. 11. AFM topography (left) and UFM (right) images in the central region at the end of an injection-moulded bar from run no. 4. No significant elongation of the rubber particles is observed.

UFM images in Figs. 8 and 11 together with the SEM micrographs of Figs. 7 and 10 verify the effect of the fountain flow phenomenon on the developed rubber-toughened microstructure during injection moulding. It is clearly shown that the particles are highly elongated in the skin region while they remain near spherical in the central region.

The same AFM and UFM investigation has been carried out for the injection moulded samples from run no. 3. Fig. 12 shows the AFM and UFM images taken on the side surface of the mouldings.

The arguments presented for the samples from run no. 4, hold for this case as well. Indeed, the rubber particles are quite elongated in the skin region. The particles display the same degree of eccentricity as those in the samples from run no. 4. Orientation of the rubber particles also follows the same pattern as before, i.e. the particles are well oriented with the melt flow direction.

Interestingly, the main difference between samples from run nos. 4 and 3 lies in the number of particles present in the skin region. Counting has revealed that on average, there are more particles present in the images from run no. 4 samples. The number of particles present in a surface of size $8 \times 8\ \mu m^2$ on the side surface of a bar from run no. 4 averaged a value of around 115. This number remained almost constant along the length of the bar, from the injection gate to the end of the flow path. On the other hand, a number of around 80 particles were typically counted in a surface of the same size on the side surface of a bar from run no. 3. Therefore, it can be assumed that there is a higher

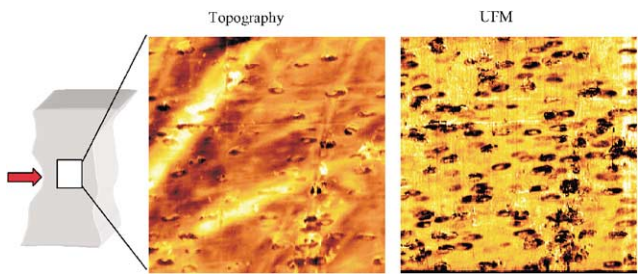

Fig. 12. AFM topography (left) and UFM (right) images on the surface of a moulding from run no. 3. The flow direction is horizontal. Elongation of the rubber particles is evident.

volume fraction of rubber in the skin region of samples from run no. 4.

Furthermore, the particles appear to be more evenly distributed along the length of sample no. 4. There are some fluctuations in the number of particles of sample no. 3 along the length of the bar. There is a tendency for the number of particles to decline from a number of around 180 very close to the injection gate to a number of about 80 in most of the rest of the surface of the bar (these numbers refer again to a scanned surface of size $8 \times 8\ \mu m^2$).

This difference in the number, orientation and distribution of particles in the skin region could contribute to the difference in mechanical properties between samples from run nos. 3 and 4. This is particularly true for the flexural properties where the properties close to the surface of the bar make the greatest contribution to the deformation. However one would expect the samples from run no. 3 to have a higher flexural modulus, since they have a lower volume fraction of rubber in the skin region, given that the rubber has a lower modulus than the acrylic. The mechanical testing and the regression analysis presented earlier have shown the opposite to be true. The extent of elongated rubber particles may induce mechanical anisotropy in these materials under the right processing conditions. Of course non-microstructural factors are expected to also play a part, in particular the residual stresses in the sample resulting from the particular moulding conditions. More research is needed to address these issues.

4. Conclusions

The design of experiments (DOE) method is a statistically sound and highly organised approach for the elucidation of the importance of processing conditions during injection moulding of rubber-toughened acrylics. Variation of the processing conditions, and of back pressure in particular, has been shown to significantly affect the mechanical properties of the mouldings. It is believed that back pressure is significant because it affects the packing and orientation of the chain molecules. Screw speed has been found to affect the flexural properties, while the interaction of barrel and mould temperatures has been found to affect the mouldings' impact strength.

SEM has shown the difference in microstructure when a sample is fractured by different methods. However it failed to show significant differences between samples produced under different conditions and fractured by the same method. The cavitation and internal debonding of the rubber particles during the impact tests (due to high loading rates) may contribute to the densely stress-whitened appearance of the specimens that have undergone impact testing.

UFM coupled with height profile analysis can reveal important information on the size, shape and distribution of the rubber particles. AFM and UFM investigation of the injection-moulded samples reveal that the rubber particles in the skin region are substantially elongated and well aligned with the melt flow. On the other hand, no significant elongation is observed in the central region of the sample at the end of the moulding. In all cases, no significant particle agglomeration was observed; the particles appear to be well dispersed in the matrix.

It has been shown that there is a higher volume fraction of rubber in the skin region of samples from run no. 4, than near the surface of samples from run no. 3. Additionally, the particles are more evenly distributed along the length of sample no. 4. These two differences between the samples from run nos. 3 and 4 could account for their respective difference in flexural properties. Nevertheless, more work is needed to establish the synergistic effect of the number and distribution of rubber particles on sample stiffness.

This work has shown that the processing history has an important effect on the mechanical properties of the moulding. Furthermore, the variation in processing conditions induces a variation to the rubber-toughened microstructure (the number and distribution of rubber particles in the skin region of the moulding), which is not detected by SEM but is discernible by UFM. In this manner, a link is established between processing history, microstructure and mechanical properties for RTPMMA mouldings.

Acknowledgments

The authors wish to thank EPSRC and INEOS Acrylics (Wilton, UK) for funding this project. Many thanks to Mr Gary Hunt, Mr Ian Dargue and Mr Jim Plows for their guidance during the injection moulding experiments and mechanical testing.

References

[1] Chiu CP, Hsieh MC. J Engng Mater Tech Trans ASME 1987;109(2):171–5.
[2] Akay M, Ozden S. Int Polym Proc 1996;11(2):179–87.
[3] Ho KC, Hwang JR, Doong JL. Polym Polym Compos 1996;4(8):563–75.
[4] Clarke GM. Introduction to the design and analysis of experiments. New York: Wiley; 1997.
[5] Hicks CR. Fundamental concepts in the design of experiments. Oxford: Oxford University Press; 1993.
[6] Montgomery DC. Design and analysis of experiments. New York: Wiley; 1997.
[7] Sawyer LC, Grubb DT. Polymer microscopy. London: Chapman & Hall; 1996.
[8] Ratner BD, Tsukruk VV. Scanning probe microscopy of polymers. ACS symp series, Washington, DC: ACS; 1998.
[9] Dinelli F. Ultrasonic force microscopy: surface elastic properties mapping and stiffness evaluation at the nanoscale level. DPhil Thesis. University of Oxford; 1999.
[10] Dinelli F, Assender HE, Takeda N, Briggs GAD, Kolosov OV. Surf Interf Anal 1999;27:562–7.

[11] Kolosov O, Yamanaka K. Jpn J Appl Phys 1993;32(8A):L1095–8.
[12] Yamanaka K, Ogiso H, Kolosov O. Appl Phys Lett 1994;64(2): 178–80.
[13] Kolosov O, Ogiso H, Tokumoto H, Yamanaka K. Nanostruct Quant Effects 1994;31:345–8.
[14] Kolosov O, Briggs A, Yamanaka K, Arnold W. Acoust Imag 1996;22: 665–8.
[15] Warren PD, Kolosov OV, Roberts SG, Briggs GAD. Nanotechnology 1996;7:288–94.
[16] Dinelli F, Biswas SK, Briggs GAD, Kolosov OV. Appl Phys Lett 1997;71(9):1177–9.
[17] Kolosov O. Mater World 1998;6(12):753–4.
[18] Dinelli F, Castell MR, Ritchie DA, Mason NJ, Briggs GAD, Kolosov OV. Philosophical Magazine A. Physics of Condensed Matter Structure Defects and Mechanical Properties 2000;80(10):2299–323.
[19] Cuberes MT, Assender HE, Briggs GAD, Kolosov OV. J Phys, Part D: Appl Phys 2000;33(19):2347–55.
[20] Rigdahl M. Internal stresses and stress relaxation in polymeric materials. PhD Thesis. Chalmers University of Technology, Goteborg; 1976.
[21] Sawhney G, Gupta SK, Misra A. J Appl Polym Sci 1996;62: 1395–405.
[22] Nadkarni VM, Jog JP. Polym Engng Sci 1987;27(6):451–7.
[23] Murphy MW, Thomas K, Bevis MJ. Plast Rubber Proc Appl 1988; 9(1):3–16.
[24] O'Donnell HJ, Baird DG. Int Polym Proc 1996;11(3):257–70.
[25] O'Donnell HJ, Baird DG. Polym Engng Sci 1996;36(7):963–78.
[26] Skourlis TP, Mohapatra B, Chassapis C, Manoochehri S. Adv Polym Technol 1997;16(2):117–28.
[27] Qiu DQ, Prentice P. Adv Polym Technol 1998;17(1):23–36.
[28] Rosato DV. Injection molding handbook. New York: Van Nostrand Reinhold Company Inc; 1986.
[29] Lovell PA, McDonald J, Saunders DEJ, Sherratt MN, Young RJ. Plast Rubber Compos Proc Appl 1991;16(1):37–44.
[30] Konzol L, Doll W, Michler GH. Colloid Polym Sci 1992;270(10): 972–81.
[31] Wu S. Polymer 1985;26(12):1855–63.
[32] Bucknall CB. Toughened plastics. Barking: Applied Science Publishers Ltd; 1977.